PCCP

PAPER

View Article Online
View Journal | View Issue

Cite this: *Phys. Chem. Chem. Phys.*, 2026, **28**, 4219

Dimer formation of 7-azaindole in phosphonium-based ionic liquids: anion-dependent behavior

Faruk Hossain, Kotaro Takahashi, Maharoof Koyakkat and Hideaki Shirota *

Received 12th November 2025,
Accepted 22nd January 2026

DOI: 10.1039/d5cp04361a

rsc.li/pccp

In this study, we have investigated the dimer formation behavior of 7-azaindole (AI) in trihexyltetradecylphosphonium ($[P_{666,14}]^+$) based ionic liquids (ILs) with seven anion species (bis(fluorosulfonyl)amide $[NF_2]^-$, bis(trifluoromethylsulfonyl)amide $[NTf_2]^-$, bis(nonafluorobutylsulfonyl)amide $[NNf_2]^-$, trifluoromethanesulfonate $[OTf]^-$, tetrafluoroborate $[BF_4]^-$, dicyanamide $[DCA]^-$, and bromide Br^-) using ^1H NMR. The physicochemical properties of the liquids, such as density, viscosity, surface tension, and electrical conductivity, as well as solvent polarity parameters (donor number DN, acceptor number AN, and π* polarity), were also characterized for all seven ILs in this study. The dimerization constant *K*, estimated from the concentration-dependent chemical shift of the proton attached to the nitrogen atom at the 7-position of AI, increases with decreasing DN of the ILs, while that is not correlated with AN and π* polarity. The relation between *K* and DN in the ILs qualitatively agrees with the behavior observed in common organic solvents. However, AI dimerization in the present ILs occurs even in ILs with higher DN than those of common organic solvents. This behavior is likely attributed to the extensive nonpolar regions formed by the nanosegregated structure of the ILs. The thermal stability and phase-transition properties of the present ILs were also characterized.

1. Introduction

Ionic liquids (ILs) are composed purely of cations and anions with melting points below 373 K.[1–7] If the melting point of an IL is below ambient temperature, it is referred to as a room temperature IL. Compared to conventional solvents, ILs possess several advantageous properties, including negligible vapor pressure under ambient temperature and pressure conditions (and are thus nonflammable or less flammable), intrinsic ionic conductivity, and a superior dissolving power toward a wide range of solutes. ILs are therefore promising as environmentally friendly and safe solvents, suitable for use as liquid materials in batteries, lubricants, separators, pharmaceutical formulations, and reaction media.[6,8–12] In addition, the molecular-level structure and interactions of ILs have been extensively studied to achieve a more comprehensive understanding of their physicochemical behavior.[13–17]

Typical cations found in ILs, such as 1-butyl-3-methylimidazolium, 1-methyl-1-hexylpyrrolidinium, and triethyloctylphosphonium, possess a relatively long alkyl group, and are therefore amphiphilic. The amphiphilic nature of the cation in ILs leads to the formation of segregated (microheterogeneous) liquid structures. Such segregated structures in ILs have been predicted through molecular dynamics (MD) simulations[18–20] and subsequently confirmed by X-ray scattering experiments.[21–23] More recently, Margulis and coworkers analyzed the structure factors of ILs in detail using MD simulations and clarified that the peaks at longer length scales are associated with polarity and charge alternations, as well as adjacency correlations between neighboring atoms.[24,25] Considering the application of ILs as reaction media, it is essential to systematically investigate reaction and solvation dynamics in segregated ILs, as well as the microenvironments surrounding solutes.[26–34]

7-Azaindole (AI) forms a dimer (Fig. 1) in the gas phase and in nonpolar solvents through cooperative hydrogen bonds (HBs). Because of its HB complex structure, the AI dimer has been extensively studied as a model system for nucleic acid base pairing. Indeed, the AI dimer became an important research system following the pioneering study by Kasha and coworkers on excited-state double proton transfer in solution.[35] In particular, the mechanism of the initial step of photoinduced double proton transfer in the AI dimer has been extensively investigated.[36–51] Although the existence/absence of the AI dimer in polar and less-polar solvents was initially unclear,[45,47,52] direct observations of vibrational modes associated with the cooperative HB complex of AI in nonpolar,[53,54] as well as less polar and polar solvents,[55] have been achieved using low-frequency spectroscopic techniques. We also demonstrated, based on ^1H NMR measurements performed by Walmsley,[56] that the dimerization constant (*K*) of AI depends on the donor number (DN), which is a scale of Lewis basicity that indicates the hydrogen-bond-accepting ability of the solvent.[55]

As mentioned above, ILs typically possess a segregated structure arising from the amphiphilic nature of their cations.[20,21,23,26]

Department of Chemistry, Chiba University, 1-33 Yayoi, Inage-ku, Chiba 263-8522, Japan. E-mail: shirota@faculty.chiba-u.jp

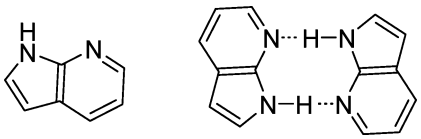

Fig. 1 Chemical formulae of AI monomer and AI dimer.

Such a complex liquid structure leads to intricate reaction and solvation dynamics in ILs.[26–34] To date, however, no studies have investigated the state or dimerization behavior of AI in ILs. In this study, we examined the dimerization constant (K) of AI in trihexyltetradecylphosphonium-based ILs ($[P_{666,14}]^+$) containing seven different anions, bis(fluorosulfonyl)amide $[NF_2]^-$, bis(trifluoromethylsulfonyl)amide $[NTf_2]^-$, bis(nonafluorobutylsulfonyl)amide $[NNf_2]^-$, trifluoromethanesulfonate $[OTf]^-$, tetrafluoroborate $[BF_4]^-$, dicyanamide $[DCA]^-$, and bromide Br^-, using ^{1}H NMR spectroscopy (Fig. 2). The primary objective of this study is to clarify the influence of anion species on the AI dimer formation behavior in phosphonium-based ILs, whose bulky alkyl-substituted cations are expected to exhibit relatively weak interactions with AI compared with the anions. In addition, we compare and discuss the differences in AI dimerization behavior between ILs and conventional solvents.

2. Experiments

2.1. Sample preparation

AI (Aldrich, 98%), betaine 30 (Aldrich, 90%), and *N*,*N*-diethyl-4-nitroaniline (DENAN; Apollo Scientific, 98%) were used without further purification. $[P_{666,14}][NF_2]$, $[P_{666,14}][NTf_2]$, $[P_{666,14}][NNf_2]$, $[P_{666,14}][OTf]$, $[P_{666,14}][BF_4]$, and $[P_{666,14}]Br$ were synthesized according to previously reported procedures for phosphonium-based ILs in our laboratory.[57,58] The purity and composition of the products were confirmed with ^{1}H NMR spectroscopy and elemental analysis ($<0.4\%$). The synthesis details of the ILs are provided in the supplementary information (SI). $[P_{666,14}][DCA]$ (Iolitec) was purified prior to use. The purity of the $[P_{666,14}][DCA]$ sample was verified by ^{1}H NMR spectroscopy ($>99\%$; Fig. S1).

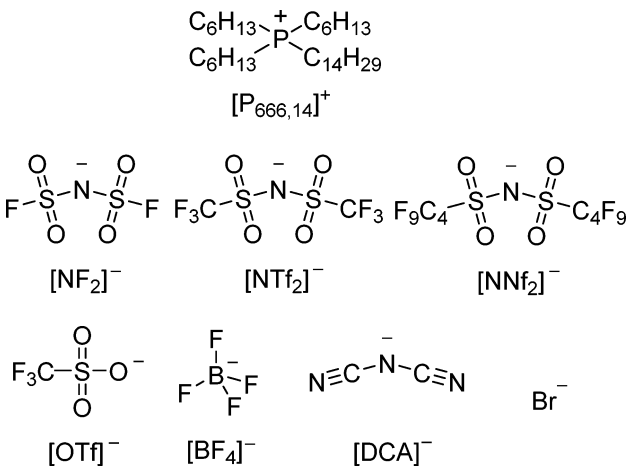

Fig. 2 Chemical formulae of cation and anions of ILs used in this study.

The purification procedure is described in detail in the SI. The water content of the ILs was determined to be <100 ppm by Karl Fischer titration using a coulometric titrator (Hiranuma AQ-300): 59.1 ppm for $[P_{666,14}][NF_2]$, 69.0 ppm for $[P_{666,14}][NTf_2]$, 77.8 ppm for $[P_{666,14}][NNf_2]$, 75.8 ppm for $[P_{666,14}][OTf]$, 96.5 ppm for $[P_{666,14}][BF_4]$, 86.9 ppm for $[P_{666,14}][DCA]$, and 59.4 ppm for $[P_{666,14}]Br$. (Acetylacetonato)(*N*,*N*,*N*′,*N*′-tetramethylethylenediamine)copper(II) perchlorate ($[Cu(acac)(tmen)][ClO_4]$) was synthesized following the procedure reported by Fukuda and Sone.[59] The product was confirmed with elemental analysis of H, C, and N ($<0.25\%$). Details of the synthetic procedures for the ILs and $[Cu(acac)(tmen)][ClO_4]$ are summarized in the SI. The ILs were dried under vacuum at 313 K for more than 36 h prior to use.

For ^{1}H NMR experiments to estimate the K values, a 1.00 mol dm^{-3} stock solution of AI in acetonitrile was used to prepare solutions with varying concentrations. First, a suitable amount of the stock solution was placed in a vial. The solution was dried under vacuum for more than 36 h at 313 K to remove the acetonitrile. Subsequently, a suitable amount of IL was added to the vial under dark conditions. The mixture was stirred overnight at 313 $\pm$ 1 K under dark conditions.

2.2. Physicochemical and thermal properties

The densities (ρ) of the neat ILs were measured at 298.0 $\pm$ 0.1 K using a vibrating-tube densitometer (Anton Paar, DMA 4100M). The viscosities (η) of the ILs were measured at 298.0 $\pm$ 0.2 K using a reciprocating electromagnetic piston viscometer (Cambridge Viscosity, ViscoLab 4100) equipped with a circulating water bath (Yamato, BB300). The electrical conductivities (σ) of the ILs were measured using a conductivity meter (Mettler Toledo, S470 SevenExcellence), and the temperature was maintained at 298.0 $\pm$ 0.2 K using a custom-built Peltier module temperature controller (VICS, VPE35-5-20TS). The surface tensions of the ILs were measured by the pendant drop method at 298.0 $\pm$ 0.2 K using a contact angle meter (Kyowa Interface Science, DMs-401), with the temperature controlled by a circulating water bath (EYELA, NBC-1210).

The thermal properties of the present ILs were measured using a differential scanning calorimetry (DSC) apparatus (Shimadzu, DSC-60 Plus). Approximately 15–20 mg of the IL was placed in an aluminum pan and sealed with an aluminum plate. The samples were cooled to 123 K and then heated to 333 K. The phase transition temperatures were determined during the second heating cycle. The scanning rate was set at 5 K min^{-1}. Solid indium was used as the calibration standard.

2.3. Solvent basicity, acidity, and π* polarity

The solvent polarity scales, Lewis basicity (donor number, DN),[60] Lewis acidity (acceptor number, AN),[61] and π* polarity (polarizability and dipolarity) values,[62] of the ILs were determined using $[Cu(acac)(tmen)][ClO_4]$, betaine 30, and DENAN, respectively. The absorption spectra of the dye solutions were recorded using a UV-vis spectrophotometer (Shimadzu UV-2700i). The temperature was maintained at 298.0 $\pm$ 0.1 K during the absorption measurements. A fused quartz cuvette with an optical length of 2 mm was

used. The absorption spectra of [Cu(acac)(tmen)][ClO_4] in several common solvents agreed well with previous reports by Sone and coworkers[59,63] and are summarized in Fig. S2 and Table S1. The correlation between the absorption peak frequency of the [Cu(acac)(tmen)][ClO_4] and the reported DN values[64] was evaluated based on the present data (Fig. S3). The absorption spectra of betaine 30 in several common solvents are summarized in Fig. S4 and Table S2. In most cases, peak wavelengths (or frequencies) of betaine 30 in several common solvents measured in this study agreed well with the reported values.[65,66] The correlation between the absorption peak frequency of the betaine 30 and the reported AN values obtained in this study is shown in Fig. S5. The absorption spectra of DENAN in several common solvents were measured (Fig. S6 and Table 3), and the correlation between the absorption peak frequency of DENAN and the π^* values obtained in this study (Fig. S7) agreed well with previously reported results.[62]

2.4. ^{1}H NMR measurements for estimation of AI dimerization constant

^{1}H NMR measurements of the AI in ILs at various concentrations were performed using a 400 MHz JEOL NMR spectrometer (JNM-ECS400) at 293.0 ± 1 K. Since the purpose of the NMR measurements in this study was to investigate the anion dependence of the chemical shift of the proton attached to the nitrogen atom at the 7-position of AI in ILs, a Shigemi external coaxial NMR tube system (SC-0010) was used. The lock solvent, DMSO-d_6 (TCI, >99.9%D), and the sample solutions were introduced into the outer and inner tubes, respectively. ^{1}H NMR measurements for each system were repeated twice to confirm the reproducibility of the concentration-dependent behavior of the chemical shift. The average was used for the value of the chemical shift. The uncertainty of the chemical shift was 0.04 ppm. The uncertainty of the chemical shift caused by the temperature variation in this study was 0.02 ppm.

3. Quantum chemistry calculations

Quantum chemistry calculations were performed to obtain the optimized geometries of the anions, AI monomer and dimer, and AI-anion clusters based on the ωB97XD/6-311++G(d,p) level of theory[67] using the Gaussian 16 program package.[68] The atomic charges of the optimized structures of anions and AI monomer and dimer were calculated through natural bond orbital analysis.[69] The interaction energies between the AI and anions were calculated using the counterpoise method.[70,71] The atomic coordinates and charges of the optimized anions, as well as those of the AI monomer and dimer, are summarized in the SI (Tables S4–S12). The atomic coordinates of the AI-anion clusters were listed in the SI (Tables S13–S19).

4. Results

4.1. Physicochemical and thermal properties of ILs

Table 1 lists the values of density (ρ), surface tension (γ), viscosity (η), and electrical conductivity (σ) of the ILs at 298.0 K, as well as their formula weights (FW). The values of the density, viscosity, and electrical conductivity of [$P_{666,14}$][NTf_2] and [$P_{666,14}$][DCA] have been previously reported by other research groups.[72,73] The values for [$P_{666,14}$][NTf_2] obtained in this study are in good agreement with the reported data.[72,73] The density and electrical conductivity values of [$P_{666,14}$][DCA] measured in this study are also in reasonable agreement with the reported values.[72,73] The viscosity value of [$P_{666,14}$][DCA] determined in this study lies between the reported values by Pozao-Gonzalo *et al.*[72] and Blanco *et al.*[73] To the best of our knowledge, the liquid properties of [$P_{666,14}$][NF_2], [$P_{666,14}$][NNf_2], [$P_{666,14}$][OTf], [$P_{666,14}$][BF_4], and [$P_{666,14}$]Br, as well as the surface tension values of [$P_{666,14}$][NTf_2] and [$P_{666,14}$][DCA], are reported here for the first time. The anion dependence of the physicochemical properties of [$P_{666,14}$]$^+$-based ILs is relatively small compared with that of typical imidazolium- and pyrrolidinium-based ILs, probably because of its relatively bulky cation.[2,74,75]

The DSC charts of the present ILs are summarized in Fig. S8. In preceding works by several groups, transitions with a small endothermic process of [$P_{666,14}$][NTf_2] and [$P_{666,14}$][DCA] were assigned to the glass transition.[76,77] Recently, Wojnarowska *et al.* assigned this process to the liquid–liquid transition based on DSC measurements at various scanning rates.[78] The DSC charts of [$P_{666,14}$][NTf_2] and [$P_{666,14}$][BF_4] obtained in this study are in good agreement with those previously reported by Wojnarowska *et al.* The thermal transitions of the present ILs were identified following the criteria reported by Wojnarowska *et al.*, and the corresponding transition temperatures are listed in Table 1. The transition temperatures of [$P_{666,14}$][NTf_2], [$P_{666,14}$][BF_4], and [$P_{666,14}$][DCA] estimated in this study are relatively well-agreed with the values reported by other groups (some of them assigned to the glass transition).[76–78]

Table 1 Densities ρ, surface tensions γ, viscosities η, and electrical conductivities σ at 298 K and liquid–liquid transition temperatures T_{LL}, cold crystallization temperatures T_c, and melting point T_m of the ILs

ILs	FW	ρ^a (g cm^{-3})	γ^b (mN m^{-1})	η^c (mPa s)	σ^c (mS cm^{-1})	$T_{LL}{}^d$ (K)	$T_c{}^d$ (K)	$T_m{}^d$ (K)
[$P_{666,14}$][NF_2]	663.43	1.0123	31.8	398.4	0.0809	195	213	256
[$P_{666,14}$][NTf_2]	763.42	1.0672	29.4	357.0	0.0745	196		
[$P_{666,14}$][NNf_2]	1064.04	1.2127	23.3	672.1	0.0265		250	290
[$P_{666,14}$][OTf]	632.46	0.9831	29.8	821.5	0.0283	201		
[$P_{666,14}$][BF_4]	570.51	0.9379	30.1	1304	0.0164		251	289
[$P_{666,14}$][DCA]	544.90	0.8981	30.4	390.0	0.0799	201	234	255
[$P_{666,14}$]Br	562.42	0.9554	30.3	2086	0.0028		251	290

^{a} ±0.1%. ^{b} ±1%. ^{c} ±3%. ^{d} ±1 K.

4.2. Polarity parameters of ILs

Solvent polarity is an important physicochemical parameter that governs solvation behavior, the microenvironment around solute molecules and solute–solvent interactions in solution. Compared with conventional molecular solvents, reports on the polarity parameters of ILs are considerably limited. To the best of our knowledge, no prior studies have reported the polarity parameters of the present ILs. Therefore, we determined three key polarity parameters (DN, AN, and π* polarity) using appropriate solvatochromic probe dyes. Notably, the present ILs possess a large cation, and thus, they are inhomogeneous compared to traditional molecular liquids. In inhomogeneous systems, a solvatochromic molecule often probes the microscopic/local region.[79] Therefore, the solvatochromic scales of the present ILs estimated in this study might be operational. However, we believe that qualitative discussion of the anion-dependent dimerization behavior based on the solvent parameter in this study is adequate, because the same cation was chosen for the present ILs.

For determining the DN, we used [Cu(acac)(tmen)][ClO_4].[59,63] Fig. 3 shows the absorption spectra of [Cu(acac)(tmen)][ClO_4] in the ILs. The absorption spectrum of [Cu(acac)(tmen)][ClO_4] varies depending on the ILs employed. For example, the absorption spectrum of [Cu(acac)(tmen)][ClO_4] in [$P_{666,14}$]Br appears at a longer wavelength, whereas that in the [$P_{666,14}$]$^+$-based ILs containing bis(perfluoroalkylsulfonyl)-amides anions appears at shorter wavelengths. The values of the absorption maxima λ_{abs} of [Cu(acac)(tmen)][ClO_4] in the ILs are listed in Table S13. The DN values were determined from λ_{abs} using a calibration line between DN and λ_{abs} using the DN values of conventional solvents[64] in this study (Table S1 and Fig. S3). The determined DN values of the ILs are listed in Table 2. Compared with most conventional solvents (Fig. S2 and Table S1), the absorption spectra of [Cu(acac)(tmen)][ClO_4] in the ILs are red-shifted, indicating that the ILs exhibit higher DN values. However, it should be noted that the DN values of typical 1-alkyl-3-methylimidazolium-based ILs and ammonium-based ILs with relatively short alkyl groups are even higher than those of the investigated phosphonium-based ILs.[80]

For determining the AN values of the ILs, betaine 30 was used as the solvatochromic probe.[80] Fig. 4 shows the absorption spectra of betaine 30 in the ILs. The absorption spectrum of betaine 30 varies depending on the IL, as well as [Cu(acac)(tmen)][ClO_4]. For example, the absorption spectrum of betaine 30 in [$P_{666,14}$]Br appears at a longer wavelength, whereas that in [$P_{666,14}$][NNf_2] appears at a shorter wavelength. The values of λ_{abs} of betaine 30 in the ILs are listed in Table S13. The AN values were determined from λ_{abs} in the ILs using a calibration line between AN and λ_{abs}, constructed from the AN data for conventional solvents[61] in this study (Table S2 and Fig. S5). The AN values of the ILs are listed in Table 2.

The π* polarity values of the ILs were determined using the solvatochromic dye DENAN.[62] Fig. 5 shows the absorption spectra of DENAN in the ILs. Unlike [Cu(acac)(tmen)][ClO_4] and betaine 30, the absorption spectra of DENAN exhibit only minor variation among the present ILs compared with those in conventional solvents (Fig. S6). The values of λ_{abs} of DENAN in

Table 2 Polarity parameters, DN, AN, and π* polarity of the ILs used in this study

ILs	DN	AN	π* polarity
[$P_{666,14}$][NF_2]	37.7	21.1	0.91
[$P_{666,14}$][NTf_2]	38.6	22.2	0.88
[$P_{666,14}$][NNf_2]	38.8	24.3	0.88
[$P_{666,14}$][OTf]	40.4	20.9	0.88
[$P_{666,14}$][BF_4]	47.9	21.5	0.87
[$P_{666,14}$][DCA]	42.5	20.2	0.91
[$P_{666,14}$]Br	50.8	18.9	0.90

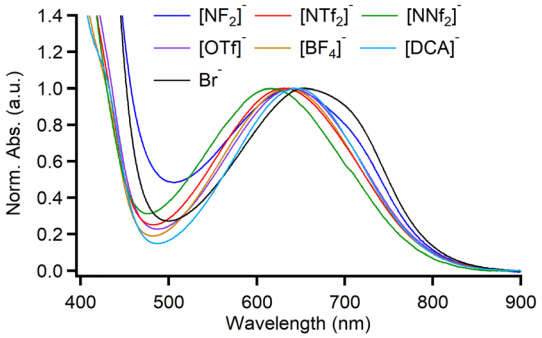

Fig. 4 Normalized absorption spectra of betaine 30 in [$P_{666,14}$]$^+$-based ILs with various anions.

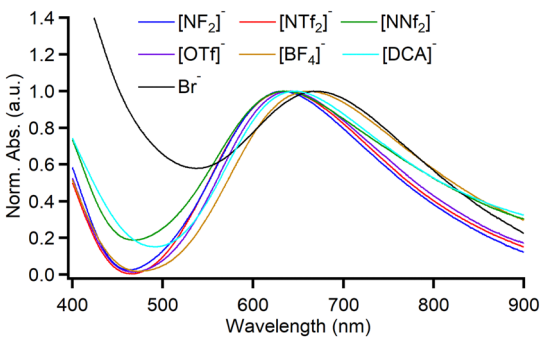

Fig. 3 Normalized absorption spectra of [Cu(acac)(tmen)][ClO_4] in [$P_{666,14}$]$^+$-based ILs with various anions.

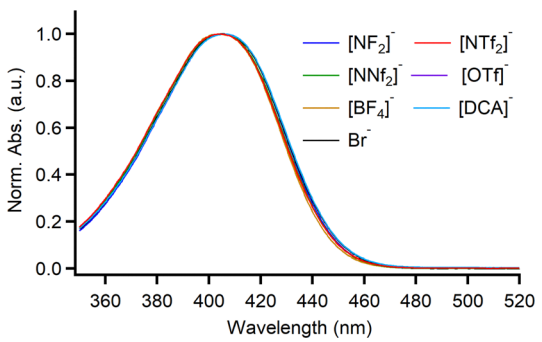

Fig. 5 Normalized absorption spectra of DENAN in [$P_{666,14}$]$^+$-based ILs with various anions.

the ILs are listed in Table S13. The π* values of the ILs were calculated from λ_{abs} using a calibration line between π* and λ_{abs} using the reported π* values of conventional solvents[62] in this study (Table S3 and Fig. S7). The determined π* values of the ILs are listed in Table 2.

4.3. Anion dependence of the dimerization constant of AI in ILs

Fig. 6 shows the concentration-dependent ^{1}H NMR spectra of the proton attached to the N at the 7-position of AI (H7N) in $[P_{666,14}][NTf_2]$, $[P_{666,14}][OTf]$, and $[P_{666,14}]Br$, as representative examples. For AI/$[P_{666,14}][NTf_2]$ and AI/$[P_{666,14}][OTf]$, the H7N proton resonance shifts downfield with increasing AI concentration. Conversely, the H7N chemical shift of AI in $[P_{666,14}]Br$ remains nearly constant regardless of AI concentration. Similar concentration-dependent behavior of the chemical shift of H7N was reported in dimethyl sulfoxide, which has a large DN (29.8).[55] Like in dimethyl sulfoxide, the H7N of AI can interact with Br^- *via* a hydrogen bond. Fig. 7 illustrates the chemical shift of H7N against the AI concentration in the present IL systems.

We analyzed the concentration dependence of the H7N chemical shift of AI in the ILs, following our previous study[55] based on the method examined by Walmsley.[56] Briefly, the *K* values for the AI/IL systems were estimated by a simple equilibrium model, which assumes that only the AI monomer and dimer species exist at equilibrium ($[AI] = [AI_1] + 2[AI_2]$, where $[AI_1]$ is the concentration of AI monomer and $[AI_2]$ is the concentration of AI dimer). *K* is given by

$$K = \frac{[AI_2]}{[AI_1]^2}. \quad (1)$$

The observed chemical shift of a proton in a rapid exchange system is the weighted average of the chemical shifts of the two species involved.[81] The present system meets this condition, since distinct peaks corresponding to the AI monomer and dimer were not observed in the spectra. Thus, the observed chemical shift is given by

$$\delta_{obs} = \frac{[AI_1]}{[AI]}\delta_1 + \frac{2[AI_2]}{[AI]}\delta_2 \quad (2)$$

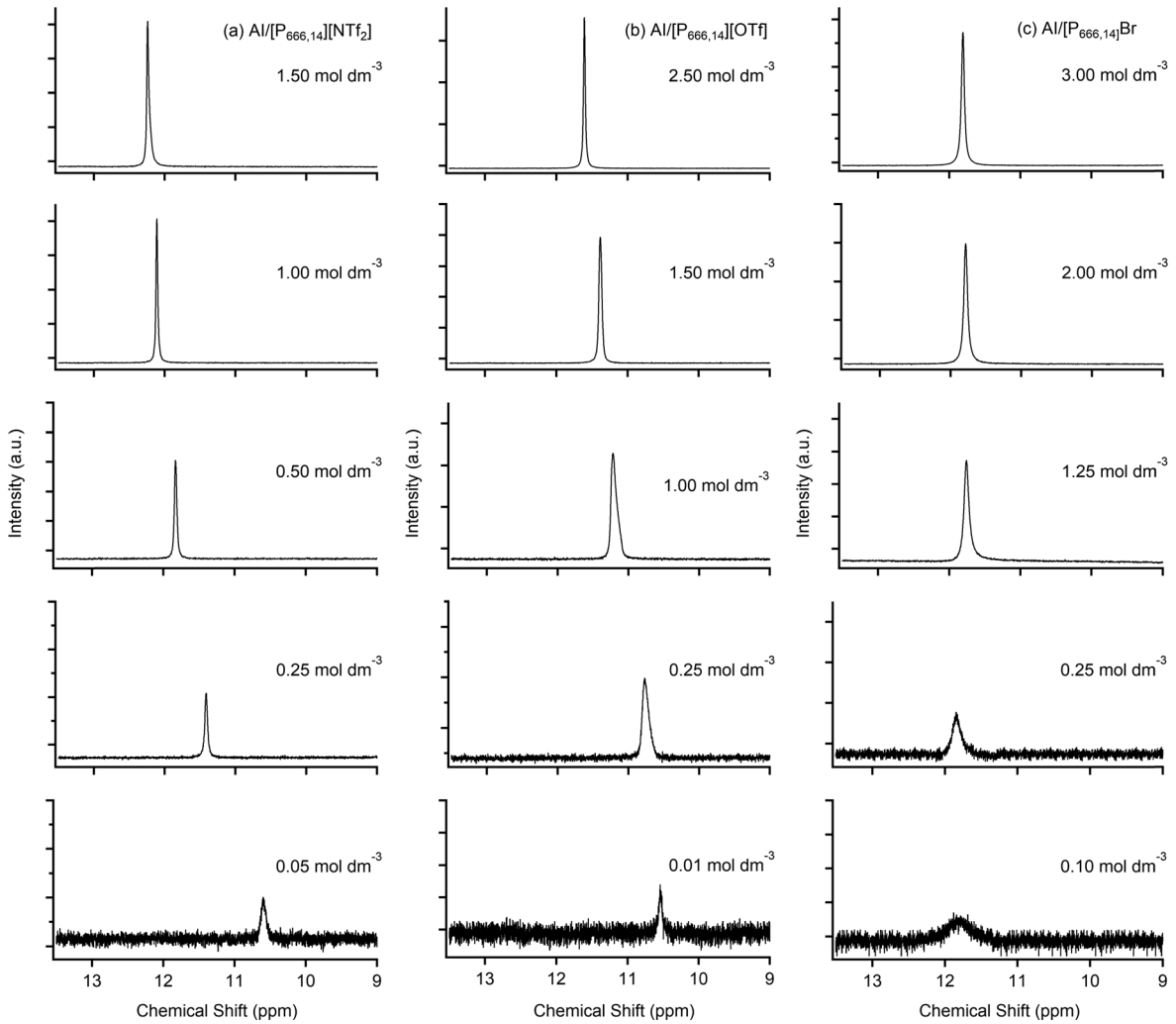

Fig. 6 Concentration-dependent NMR spectral band of the proton attached to the N at the 7-position of AI in (a) $[P_{666,14}][NTf_2]$, (b) $[P_{666,14}][OTf]$, and (c) $[P_{666,14}]Br$.

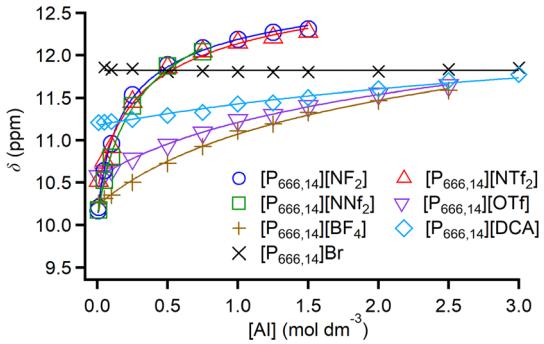

Fig. 7 Concentration-dependent chemical shifts of the proton attached to the N at the 7-position of Al in $[P_{666,14}]^+$-based ILs with various anions. Fits by eqn 3 are also shown. Black line for $[P_{666,14}]Br$ denotes the average.

where δ is the chemical shift in ppm and the subscripts obs, 1, and 2 denote observed, monomer, and dimer, respectively. Each solvent-dependent chemical shift of H7N can thus be fitted by

$$\delta_{obs} = \frac{\sqrt{1+8K[Al]}-1}{4K[Al]}\delta_1 + \frac{\left(\sqrt{1+8K[Al]}-1\right)^2}{8K[Al]}\delta_2. \quad (3)$$

Fig. 7 also shows fitted curves obtained using eqn (3), except for Al/$[P_{666,14}]Br$. As shown in the figure, the fitted results using eqn (3) accurately reproduce the experimental relationship between the H7N chemical shift and the Al concentration in the present IL systems, except for Al/$[P_{666,14}]Br$, which exhibited no concentration dependence of the H7N chemical shift. The values of K, δ_1, and δ_2 for Al in ILs are summarized in Table 3. Note that the δ_2 value for Al/$[P_{666,14}][DCA]$ was fixed at 13.60, corresponding to the average δ_2 value of the other systems (excluding Al/$[P_{666,14}]Br$, since the K value for Al/$[P_{666,14}][DCA]$ was minimal). Because no concentration dependence of the H7N chemical shift was observed in Al/$[P_{666,14}]Br$, the average chemical shift was defined as δ_1, indicating that Al likely exists as the monomer bound with bromide anion *via* HB.

The concentration is not small in the high-concentration region ($\sim$1 mol dm^{-3}) of this study, and thus, higher-order aggregations might exist. However, a multiple-step behavior caused by the existence of an extra component was not confirmed in the present sample, as shown in Fig. 7. In addition, this experiment probes the H7N of Al by ^{1}H NMR. Thus, unless the higher-order aggregations do not break the cooperative hydrogen-bonds or the chemical shift of the H7N is influenced by higher-order aggregations, the present experiments likely estimate the monomer–dimer system specifically. In other words, proving the H7N of Al would not be very sensitive to higher-order aggregation. Notably, the K becomes plateaued with increasing the concentration, and the Al in $[P_{666,14}]Br$ system showed no clear concentration dependence of the chemical shift even up to 3.0 mol dm^{-3}. Furthermore, the orientational relaxation due to higher-order aggregations of Al in conventional solvents at high concentrations (over $\sim$1 mol dm^{-3}) was not observed.[54,55] Thus, we believe that we are tracking the monomer and dimer in this study.

4.4. Atomic charges of anions

Because HBs occur at specific atomic sites with a large electronegativity, such as oxygen, nitrogen, or fluorine, the atomic charges of the anions were calculated using quantum chemical methods. The atomic charge distributions of the anions and Al, optimized at the ωB97XD/6-311G(d,p)++ level of theory, are exhibited in Fig. 8. The atomic charge values of the most and second-most negatively charged atoms in each anion are summarized in Table 4. For $[NF_2]^-$, $[NTf_2]^-$, and $[NNf_2]^-$, the

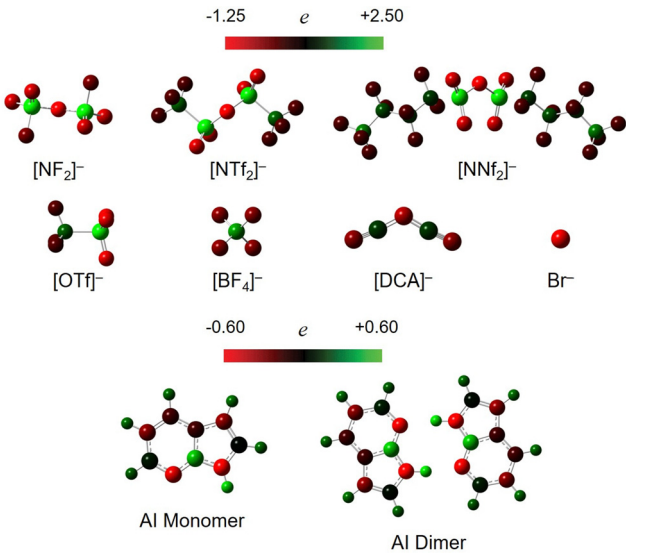

Fig. 8 Atomic charges of anions and Al optimized at the ωB97XD/6-311++G(d,p) level of theory based on the natural bond population analysis.

Table 3 Dimerization constants K and chemical shift parameters δ_1 and δ_2 obtained by the concentration-dependent chemical shift of the proton at H7N of Al in ILs by ^{1}H NMR

Systems	K (dm^3 mol^{-1})	δ_1 (ppm)	δ_2 (ppm)
Al/$[P_{666,14}][NF_2]$	2.98 ± 0.27	10.05 ± 0.03	13.26 ± 0.06
Al/$[P_{666,14}][NTf_2]$	1.60 ± 0.35	10.39 ± 0.06	13.42 ± 0.16
Al/$[P_{666,14}][NNf_2]$	1.70 ± 0.35	10.04 ± 0.06	13.82 ± 0.24
Al/$[P_{666,14}][OTf]$	0.173 ± 0.015	10.56 ± 0.01	13.63 ± 0.13
Al/$[P_{666,14}][BF_4]$	0.198 ± 0.026	10.23 ± 0.02	13.85 ± 0.03
Al/$[P_{666,14}][DCA]$	0.0643 ± 0.0040	11.18 ± 0.01	13.60[a]
Al/$[P_{666,14}]Br$	—	11.82 ± 0.02	—

[a] Fixed.

Table 4 Most and second-most negative atoms and their charges of anions optimized at the ωB97XD/6-311++G(d,p) level of theory based on the natural bond population analysis

Anions	Most negative atom	Charge (e$^-$)	Second-most negative atom	Charge (e$^-$)
$[NF_2]^-$	N	−1.184	O	−0.906
$[NTf_2]^-$	N	−1.228	O	−0.926
$[NNf_2]^-$	N	−1.218	O	−0.918
$[OTf]^-$	O	−0.983	F	−0.370
$[BF_4]^-$	F	−0.584	—	—
$[DCA]^-$	N(center)	−0.758	N(edge)	−0.589
Br^-	Br	−1	—	—

nitrogen atom bears the highest negative charge in each anion, followed by the oxygen atoms, which are the second most negatively charged. In $[DCA]^-$, all nitrogen atoms are negatively charged, but the central nitrogen atom carries a less negative charge than the terminal nitrogen atoms. Fluorine atoms in $[OTf]^-$ are also negatively charged, but their magnitude is less negative than that of the nitrogen or oxygen atoms.

4.5. Interaction energies of AI-anion clusters

Optimized AI-anion clusters at the ωB97XD/6-311++G(d,p) level of theory are shown in Fig. 9. The stabilized structures of AI-anion clusters, except for AI-Br^-, show the two sites to interact: the proton attached to the nitrogen atom at the 7-position and the proton attached to the carbon atom at the 6-position of AI. As seen in Fig. 6, these protons are positively charged. The interaction energies of the AI-anion clusters, as well as AI dimer, are listed in Table 5. The interaction energies of the AI clusters with $[OTf]^-$, $[BF_4]^-$, and Br^- are similar to that of AI dimer, but those of the AI clusters with the other anions are less negative than that of AI dimer.

5. Discussion

5.1. Comparisons with solvent parameters

Fig. 6 and 7 and Table 3 show that the *K* of AI in the phosphonium-based ILs depends on the anion species. The DN and AN values of the ILs vary depending on the anion species, whereas the π* polarity value of the present ILs shows little dependence on the anion. The minimal variation in the π* polarity values of the present ILs is likely due to the phosphonium cation, which contains relatively long alkyl groups. We therefore conclude that the π* polarity value is not a key factor governing AI dimerization in the ILs. Here, we focus on the correlations of *K* with DN and AN.

Fig. 10 presents the plots of *K vs.* DN and AN for the AI in the ILs. The relationship between *K* and DN fits well with an exponential function (or maybe a linear function up to DN = ~40), while the plots of *K* and AN were scattered. The trend between *K* and DN in the present AI/phosphonium-based ILs is

Table 5 Interaction energies of AI–anion clusters optimized at the ωB97XD/6-311++G(d,p) level of theory

	Interaction energies (kcal mol^{-1})
AI–$[NF_2]^-$	−13.13
AI–$[NTf_2]^-$	−13.60
AI–$[NNf_2]^-$	−14.18
AI–$[OTf]^-$	−17.54
AI–$[BF_4]^-$	−17.42
AI–$[DCA]^-$	−14.94
AI–Br^-	−18.25
AI–AI	−17.98

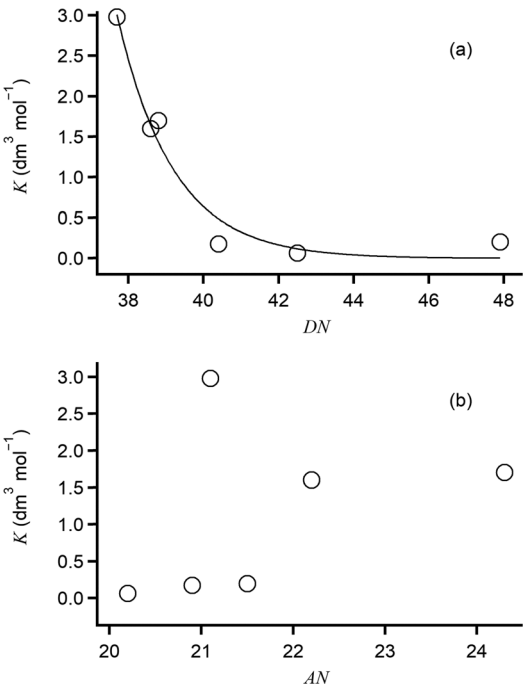

Fig. 10 Plots of *K vs.* (a) DN and (b) AN for AI in ILs. An exponential fit is also shown for DN.

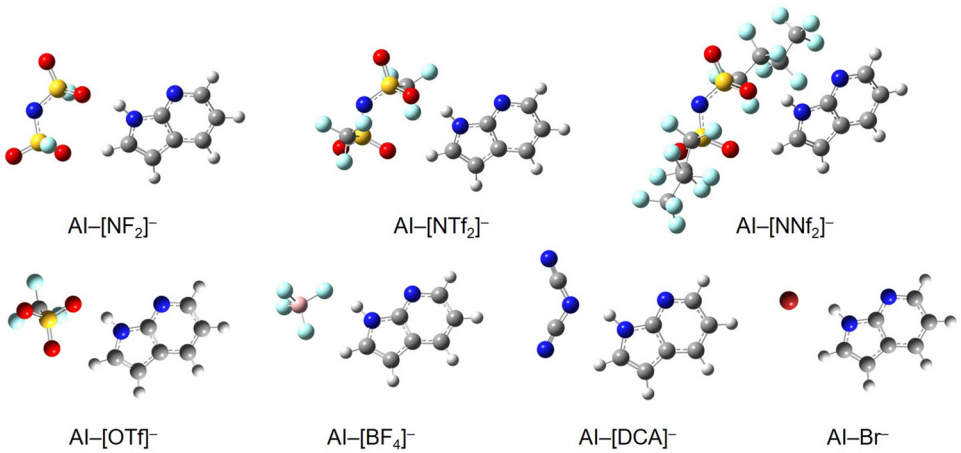

Fig. 9 AI–anion clusters optimized at the ωB97XD/6-311++G(d,p) level of theory.

consistent with that observed in conventional solvents:[55] A smaller DN value corresponds to a larger *K*. Thus, the dimer formation of AI in the ILs is significantly influenced by the Lewis basicity rather than Lewis acidity, similar to the behavior observed in conventional organic solvents.

As seen in Table 2, the DN values of the present ILs are larger than those of conventional organic solvents. For example, the DN values of methylene chloride, chloroform, acetone, acetonitrile, and DMSO are 1, 4, 17.0, 14.1, and 29.8, respectively.[82] The *K* values of AI in methylene chloride, chloroform, acetone, and acetonitrile are 14.7, 13.3, 0.727, and 0.910 $dm^3\ mol^{-1}$, respectively, and no AI dimer formation occurs in DMSO.[55] Thus, it is evident that AI dimer formation tends to occur in a medium with a higher Lewis basicity in the case of the present ILs than in conventional organic solvents.

ILs containing long alkyl groups exhibit segregated structures due to the coexistence of nonpolar and polar (ionic) regions. In the present phosphonium-based ILs, the nonpolar region predominates in the liquid because the cationic alkyl groups are long. Because the AI dimer (permanent dipole moment of 0 D based on the ωB97XD/6-311++G(d,p) level of theory) is less polar than the AI monomer (dipole moment of 1.617 D), the AI dimer is likely to reside in the nonpolar region. Thus, dimerization can occur even in media with a high Lewis basicity (DN $< \sim 40$), such as the present ILs, *e.g.*, $[P_{666,14}][NF_2]$, $[P_{666,14}][NTf_2]$, and $[P_{666,14}][NNf_2]$.

5.2. Comparison with atom charges

A highly negatively charged atom in an anion tends to interact with a hydrogen atom attached to a large electronegativity atom of a HB donor molecule. Therefore, AI in an IL containing an anion with a highly negative atomic site is expected to exist primarily as a monomer. Thus, it is useful to compare the *K* values of AI in ILs with the degree of negative charge on the most negatively charged atom of each anion species.

As shown in Table 4, the order of the anion species according to the magnitude of negativity of the most negative constituent atom is: $[NTf_2]^- > [NNf_2]^- > [NF_2]^- > Br^- > [OTf]^- > [DCA]^- > [BF_4]^-$. On the other hand, the order of the *K* values of AI in ILs, except for $[P_{666,14}]Br$, shown in Table 3 is: $[P_{666,14}][NNf_2] > [P_{666,14}][NF_2] > [P_{666,14}][NTf_2] \gg [P_{666,14}][BF_4] > [P_{666,14}][OTf] > [P_{666,14}][DCA]$. Therefore, the degree of negative charge on the constituent atoms of the anions does not directly correlate with the *K* values. In particular, $[NF_2]^-$, $[NTf_2]^-$, and $[NNf_2]^-$, possess large negativity atoms, the AI/$[P_{666,14}][NF_2]$, AI/$[P_{666,14}][NTf_2]$, and AI/$[P_{666,14}][NNf_2]$ systems exhibit relatively large *K* values. The reason why the AI/$[P_{666,14}][NF_2]$, AI/$[P_{666,14}][NTf_2]$, and AI/$[P_{666,14}]$-$[NNf_2]$ systems exhibit relatively large *K* values cannot be explained solely in terms of atomic charge. However, the comparison with the polarity parameters indicates that DN is a more reliable reporter of the *K* value of AI than the atomic-level property of charge.

5.3. Comparison with interaction energy

As seen in Table 5, the interaction energy of the AI dimer is nearly the same as that of the AI clusters with $[OTf]^-$, $[BF_4]^-$, and Br^-, which is well correlated to the trend of *K* shown in Table 3. Fig. 11 shows the plots of *K vs.* interaction energy for AI–anion clusters optimized at the ωB97XD/6-311++G(d,p) level of theory. Notably, the datum of AI–Br^- is not plotted, since its *K* cannot be estimated because of its no-concentration dependence of the chemical shift of H7N. An exponential fit is also shown for a guide to the eye. The relationship between *K* and the interaction energy is qualitatively similar to that with DN (Fig. 10a), though the positive and negative directions of the scales of the interaction energy and DN are different. By comparing the values of the interaction energy and DN, the interaction energy of the AI cluster with $[DCA]^-$ might be weakly estimated. Further examination using different cation-based ILs is promising to clarify which parameter is more appropriate.

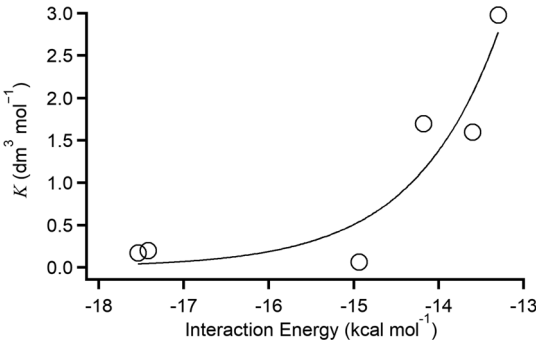

Fig. 11 Plots of *K vs.* interaction energy for AI–anion clusters optimized at the ωB97XD/6-311++G(d,p) level of theory.

6. Summary

In this study, we determined the *K* values of AI in $[P_{666,14}][NF_2]$, $[P_{666,14}][NTf_2]$, $[P_{666,14}][NNf_2]$, $[P_{666,14}][OTf]$, $[P_{666,14}][BF_4]$, $[P_{666,14}][DCA]$, and $[P_{666,14}]Br$ based on the concentration dependence of the chemical shift of H7N of AI in the ILs, as measured by ^1H NMR spectroscopy. The liquid properties, including density, viscosity, surface tension, and electrical conductivity, and polarity parameters, such as DN, AN, and π*, and thermal properties of the ILs were also characterized. Notably, the solvent polarity parameters of the seven ILs were determined for the first time in this study, and many of their liquid properties are newly reported. The dimerization constant *K* of AI in the present ILs correlates inversely with the DN: a smaller DN provides a larger *K*. This relationship between *K* and DN in the present ILs qualitatively agrees with that previously observed in conventional organic solvents. However, *K* of AI in the ILs remains large even when the DN value is as high as $\sim$38, a condition under which dimer formation does not typically occur in conventional solvents. This behavior is likely due to the extensive nonpolar regions formed by the long alkyl groups of the phosphonium cation in the ILs. Future work will focus on investigating AI dimerization in ILs with different cationic species.

Conflicts of interest

There are no conflicts to declare.

Data availability

The data supporting this article have been included as part of the supplementary information (SI). Supplementary information: sample preparation details, characterizations of solvatochromic dyes, quantum chemistry calculation results (atomic coordinates and atomic charges), and DSC charts are summarized. See DOI: https://doi.org/10.1039/d5cp04361a.

Acknowledgements

We thank Professor Katsuhiko Moriyama (Chiba University) for his kind help with NMR measurements. This work was partially supported by JSPS KAKENHI (JP22H02028 and JP25K01723). FH also thanks the Kyoritsu International Foundation for the scholarship.

References

1 J. S. Wilkes and M. J. Zaworotko, *J. Chem. Soc., Chem. Commun.*, 1992, 965–967.
2 *Ionic Liquids in Synthesis*, ed P. Wasserscheid and T. Welton, Wiley-VCH, Weinheim, 2008.
3 *Electrochemical Aspects of Ionic Liquids*, ed H. Ohno, Wiley-Interscience, Hoboken, 2005.
4 D. R. MacFarlane, M. Kar and J. M. Pringle, *Fundamentals of Ionic Liquids*, Wiley-VCH, Weinheim, 2017.
5 M. J. Earle and K. R. Seddon, *Pure Appl. Chem.*, 2000, **72**, 1391–1398.
6 J. S. Wilkes, *J. Mol. Catal.*, 2004, **214**, 11–17.
7 S. A. Forsyth, J. M. Pringle and D. R. MacFarlane, *Aust. J. Chem.*, 2004, **57**, 113–119.
8 T. Welton, *Chem. Rev.*, 1999, **99**, 2071–2083.
9 W. L. Hough and R. D. Rogers, *Bull. Chem. Soc. Jpn.*, 2007, **80**, 2262–2269.
10 N. V. Plechkova and K. R. Seddon, *Chem. Soc. Rev.*, 2008, **37**, 123–150.
11 M. Armand, F. Endres, D. R. MacFarlane, H. Ohno and B. Scrosati, *Nat. Mater.*, 2009, **8**, 621–629.
12 M. Watanabe, M. L. Thomas, S. Zhang, K. Ueno, T. Yasuda and K. Dokko, *Chem. Rev.*, 2017, **117**, 7190–7239.
13 K. Iwata, H. Okajima, S. Saha and H.-O. Hamaguchi, *Acc. Chem. Res.*, 2007, **40**, 1174–1181.
14 E. W. Castner, Jr., C. J. Margulis, M. Maroncelli and J. F. Wishart, *Annu. Rev. Phys. Chem.*, 2011, **62**, 85–105.
15 K. Fumino, S. Reimann and R. Ludwig, *Phys. Chem. Chem. Phys.*, 2014, **16**, 21903–21929.
16 R. Hayes, G. G. Warr and R. Atkin, *Chem. Rev.*, 2015, **115**, 6357–6426.
17 V. H. Paschoal, L. F. O. Faria and M. C. C. Ribeiro, *Chem. Rev.*, 2017, **117**, 7053–7112.
18 Y. Wang and G. A. Voth, *J. Am. Chem. Soc.*, 2005, **127**, 12192–12193.
19 Y. Wang and G. A. Voth, *J. Phys. Chem. B*, 2006, **110**, 18601–18608.
20 J. N. A. Canongia Lopes and A. A. H. Padua, *J. Phys. Chem. B*, 2006, **110**, 3330–3335.
21 A. Triolo, O. Russina, H.-J. Bleif and E. Di Cola, *J. Phys. Chem. B*, 2007, **111**, 4641–4644.
22 A. Triolo, O. Russina, B. Fazio, G. B. Appetecchi, M. Carewska and S. Passerini, *J. Chem. Phys.*, 2009, **130**, 164521.
23 O. Russina, A. Triolo, L. Gontrani and R. Caminiti, *J. Phys. Chem. Lett.*, 2012, **3**, 27–33.
24 H. V. R. Annapureddy, H. K. Kashyap, P. M. D. Biase and C. J. Margulis, *J. Phys. Chem. B*, 2010, **114**, 16838–16846.
25 H. K. Kashyap, J. J. Hettige, H. V. R. Annapureddy and C. J. Margulis, *Chem. Commun.*, 2012, **48**, 5103–5105.
26 J. C. Araque, J. J. Hettige and C. J. Margulis, *J. Phys. Chem. B*, 2015, **119**, 12727–12740.
27 Z. H. Hu and C. J. Margulis, *Proc. Natl. Acad. Sci. U. S. A.*, 2006, **103**, 831–836.
28 H. Jin, X. Li and M. Maroncelli, *J. Phys. Chem. B*, 2007, **111**, 13473–13478.
29 E. W. Castner, Jr., J. F. Wishart and H. Shirota, *Acc. Chem. Res.*, 2007, **40**, 1217–1227.
30 A. Samanta, *J. Phys. Chem. Lett.*, 2010, **1**, 1557–1562.
31 C. Nese and A.-N. Unterreiner, *Phys. Chem. Chem. Phys.*, 2010, **12**, 1698–1708.
32 Y. Nagasawa, *J. Photochem. Photobiol., C*, 2011, **12**, 31–45.
33 X.-X. Zhang, M. Liang, N. P. Ernsting and M. Maroncelli, *J. Phys. Chem. B*, 2013, **117**, 4291–4304.
34 K. Fujii and Y. Kimura, *Chem. Rec.*, 2023, **23**, e202200242.
35 C. A. Taylor, M. A. El-Bayoumi and M. Kasha, *Proc. Natl. Acad. Sci. U. S. A.*, 1969, **63**, 253–260.
36 K. C. Ingham, M. Abu-Elgheit and M. A. El-Bayoumi, *J. Am. Chem. Soc.*, 1971, **93**, 5023–5025.
37 K. C. Ingham and M. A. El-Bayoumi, *J. Am. Chem. Soc.*, 1974, **96**, 1674–1682.
38 K. Fuke, H. Yoshiuchi and K. Kaya, *J. Phys. Chem.*, 1984, **88**, 5840–5844.
39 K. Fuke and K. Kaya, *J. Phys. Chem.*, 1989, **98**, 614–621.
40 S. Takeuchi and T. Tahara, *J. Phys. Chem. A*, 1998, **102**, 7740–7753.
41 S. Takeuchi and T. Tahara, *Proc. Natl. Acad. Sci. U. S. A.*, 2007, **104**, 5285–5290.
42 J. Catalán, J. C. Del Valle and M. Kasha, *Proc. Natl. Acad. Sci. U. S. A.*, 1999, **96**, 8338–8343.
43 J. Catalan, P. Perez, J. C. del Valle, J. L. G. de Paz and M. Kasha, *Proc. Natl. Acad. Sci. U. S. A.*, 2002, **99**, 5793–5798.
44 A. Douhal, S. K. Kim and A. H. Zewail, *Nature*, 1995, **378**, 260–263.
45 O.-H. Kwon and A. H. Zewail, *Proc. Natl. Acad. Sci. U. S. A.*, 2007, **104**, 8703–8708.
46 D. E. Folmer, E. S. Wisniewski, S. M. Hurley and A. W. Castleman Jr., *Proc. Natl. Acad. Sci. U. S. A.*, 1999, **96**, 12980–12986.
47 J. R. Dwyer, J. Dreyer, E. T. J. Nibbering and T. Elsaesser, *Chem. Phys. Lett.*, 2006, **432**, 146–151.
48 H. Sekiya and K. Sakota, *J. Photochem. Photobiol., C*, 2008, **9**, 81–91.
49 H. Ishikawa, H. Yabuguchi, Y. Yamada, A. Fujihara and K. Fuke, *J. Phys. Chem. A*, 2010, **114**, 3199–3206.
50 M. Mukherjee, B. Bandyopadhyay and T. Chakraborty, *Chem. Phys. Lett.*, 2012, **543**, 74–79.

51 M. Mukherjee, S. Karmakar and T. Chakraborty, *J. Phys. Chem. A*, 2012, **116**, 9888–9896.
52 J. Catalan, *Proc. Natl. Acad. Sci. U. S. A.*, 2008, **105**, E78.
53 A. M. Fedor and T. M. Korter, *Chem. Phys. Lett.*, 2006, **429**, 406–409.
54 T. Kato and H. Shirota, *J. Chem. Phys.*, 2011, **134**, 164504.
55 H. Shirota, T. Fukuda and T. Kato, *J. Phys. Chem. B*, 2013, **117**, 16196–16205.
56 J. A. Walmsley, *J. Phys. Chem.*, 1981, **85**, 3181–3187.
57 H. Shirota, H. Fukazawa, T. Fujisawa and J. F. Wishart, *J. Phys. Chem. B*, 2010, **114**, 9400–9412.
58 H. Shirota, K. Takahashi, M. Ando and S. Kakinuma, *J. Chem. Eng. Data*, 2019, **64**, 4701–4707.
59 Y. Fukuda and K. Sone, *Bull. Chem. Soc. Jpn.*, 1972, **45**, 465–469.
60 V. Gutmann, *Coord. Chem. Rev.*, 1976, **18**, 225–255.
61 U. Mayer, V. Gutmann and W. Gerger, *Monatsh. Chem.*, 1975, **106**, 1235–1257.
62 M. J. Kamlet, J. L. M. Abboud, M. H. Abraham and R. W. Taft, *J. Org. Chem.*, 1983, **48**, 2877–2887.
63 R. W. Soukup and K. Sone, *Bull. Chem. Soc. Jpn.*, 1987, **60**, 2286–2288.
64 S. Glikberg and Y. Marcus, *J. Sol. Chem.*, 1983, **12**, 255–270.
65 V. G. Machado and C. Machado, *J. Chem. Educ.*, 2001, **78**, 649–651.
66 R. Pandian, H. Burda, I. Alfurayj, C. Reichardt and C. Burda, *J. Phys. Chem. B*, 2024, **128**, 6990–7001.
67 J.-D. Chai and M. Head-Gordon, *Phys. Chem. Chem. Phys.*, 2008, **10**, 6615–6620.
68 M. J. Frisch, G. W. Trucks, H. B. Schlegel, G. E. Scuseria, M. A. Robb, J. R. Cheeseman, G. Scalmani, V. Barone, G. A. Petersson, H. Nakatsuji, X. Li, M. Caricato, A. V. Marenich, J. Bloino, B. G. Janesko, R. Gomperts, B. Mennucci, H. P. Hratchian, J. V. Ortiz, A. F. Izmaylov, J. L. Sonnenberg, D. Williams-Young, F. Ding, F. Lipparini, F. Egidi, J. Goings, B. Peng, A. Petrone, T. Henderson, D. Ranasinghe, V. G. Zakrzewski, J. Gao, N. Rega, G. Zheng, W. Liang, M. Hada, M. Ehara, K. Toyota, R. Fukuda, J. Hasegawa, M. Ishida, T. Nakajima, Y. Honda, O. Kitao, H. Nakai, T. Vreven, K. Throssell, J. J. A. Montgomery, J. E. Peralta, F. Ogliaro, M. J. Bearpark, J. J. Heyd, E. N. Brothers, K. N. Kudin, V. N. Staroverov, T. A. Keith, R. Kobayashi, J. Normand, K. Raghavachari, A. P. Rendell, J. C. Burant, S. S. Iyengar, J. Tomasi, M. Cossi, J. M. Millam, M. Klene, C. Adamo, R. Cammi, J. W. Ochterski, R. L. Martin, K. Morokuma, O. Farkas, J. B. Foresman and D. J. Fox, *Gaussian 16*, Gaussian, Inc., Wallingford, CT, 2016.
69 E. D. Glendening, A. E. Reed, J. E. Carpenter and F. Weinhold, *NBO Version 3.1.*, Gaussian Inc., Pittsburgh, 2003.
70 S. F. Boys and F. Bernardi, *Mol. Phys.*, 1970, **19**, 553–566.
71 S. Simon, M. Duran and J. J. Dannenberg, *J. Chem. Phys.*, 1996, **105**, 11024–11031.
72 C. Pozo-Gonzalo, P. C. Howlett, J. L. Hodgson, L. A. Madsen, D. R. MacFarlane and M. Forsyth, *Phys. Chem. Chem. Phys.*, 2014, **16**, 25062–25069.
73 D. Blanco, M. Bartolomee, B. Ramajo, J. L. Viesca, R. Gonzalez and A. H. N. Battez, *Ind. Eng. Chem. Res.*, 2016, **55**, 9594–9602.
74 H. Shirota, S. Kakinuma, K. Takahashi, A. Tago, H. Jeong and T. Fujisawa, *Bull. Chem. Soc. Jpn.*, 2016, **89**, 1106–1128.
75 H. Shirota, M. Ando, K. Takahashi and S. Kakinuma, *Bull. Chem. Soc. Jpn.*, 2020, **93**, 1520–1539.
76 R. E. D. Sesto, C. Corley, A. Robertson and J. S. Wilkes, *J. Organomet. Chem.*, 2005, **690**, 2536–2542.
77 G. Annat, M. Forsyth and D. R. MacFarlane, *J. Phys. Chem. B*, 2012, **116**, 8251–8258.
78 Z. Wojnarowska, S. Cheng, B. Yao, M. Swadzba-Kwasny, S. McLaughlin, A. McGrogan, Y. Delavoux and M. Paluch, *Nat. Commun.*, 2022, **13**, 1342.
79 C. D. Grant, M. R. DeRitter, K. E. Steege, T. A. Fadeeva and E. W. Castner, *Langmuir*, 2005, **21**, 1745–1752.
80 C. Reichardt, *Green Chem.*, 2005, **7**, 339–351.
81 E. D. Becker, *High Resolution NMR*, Academic Press, New York, 2nd edn, 1980.
82 Y. Marcus, *J. Sol. Chem.*, 1984, **13**, 599–624.

